COST-EFFICIENT OPTIMIZATION OF SYNTHETIC MOORING SYSTEMS WITH POLYMER SPRINGS FOR 15 MW FLOATING WIND TURBINES IN SHALLOW WATERS

Salvatore Verde[1], Eduardo Nobre Lages[2]
[1]Professor, Universidade Federal de Alagoas, Delmiro Gouveia, Brazil
salvatore.verde@delmiro.ufal.br
[2]Professor, Universidade Federal de Alagoas, Maceió, Brazil
enl@ctec.ufal.br

ABSTRACT

The deployment of larger wind turbines has significantly reduced energy costs but has also introduced new challenges for installations in intermediate water depths (50–150 m), where efficient mooring systems are critical. While traditional chain catenary arrangements and polyester-based solutions are widely used, they often fail to adequately mitigate peak loads or maintain platform pitch control, particularly under extreme environmental conditions. Nylon has emerged as a promising mooring material due to its inherent elasticity, which effectively reduces peak loading. However, its use can lead to increased platform pitch and may raise concerns about long-term fatigue performance. To address these issues, recent optimization frameworks have focused on hybrid nylon-chain systems, fine-tuning parameters such as line length and diameter. The integration of Load Reduction Devices (LDRs), tailored in length, target load, and stiffness, further enhances mooring performance by mitigating peak loads and fatigue damage while preserving platform stability and compliance. In this study, an LDR-nylon-chain mooring system was optimized to minimize both LDR length and target load across various platform radii. The resulting configurations achieved substantial cost reductions without compromising motion performance requirements. Minor adjustments were required to ensure compliance with tension limits, and subsequent analyses revealed pronounced peaks in the system's power spectrum—attributed to the LDR's low damping characteristics—thus highlighting an area that warrants further refinement. Overall, this work provides valuable insights for designing cost-effective and reliable mooring systems in shallow water environments, thereby advancing safe and economical floating wind technology.

KEYWORDS: *Floating wind turbine, Mooring systems, Nylon rope, Genetic algorithm optimization, Spring polymer.*

I. INTRODUCTION

As governments worldwide aim for net-zero emissions by the mid-21st century, the renewable energy sector continues to expand into offshore areas with floating offshore wind technology, highlighting the pivotal role of wind energy. Offshore wind capacity currently stands at 64.3 GW, representing 7% of global wind energy. The Global Wind Energy Council (GWEC) forecasts an increase of over 380 GW by 2032, reaching a total capacity of 447 GW [1]. For instance, Brazil's Offshore Support System [2] manages areas with a potential of 700 GW in waters up to 100 m deep [3], where floating offshore wind turbines (FOWTs) are favoured over fixed-bottom designs. FOWTs are connected to the seabed using mooring lines and anchors. Increasing turbine sizes is essential for cost reduction; however, this scaling poses challenges to floating structures and mooring systems. The costs associated with mooring systems largely depend on two main factors: the minimum breaking load (MBL) of the mooring lines and the anchor's capacity to withstand extreme peak loads. Reducing these loads involves decreasing system stiffness or increasing compliance, which can be achieved through geometric means (e.g., catenary chains) or elastic means (e.g., taut synthetic ropes).

Maximizing compliance while still meeting displacement codes reduces peak loads and allows for more cost-effective designs. In deep waters, catenary and taut systems naturally offer compliance through long suspended lines. However, in shallow waters, catenary systems require heavier lines to achieve the necessary pretension. These heavier lines increase stiffness, footprint, and peak loads, rendering them less economical [4]. Taut systems using polyester ropes reduce line costs but increase anchor costs due to vertical loads; moreover, large peak loads and platform pitch remain significant issues [5]. Nylon ropes can effectively reduce peak and anchor loads but do not fully address problems related to platform pitch and fatigue life [6].

Load Reduction Devices (LDRs) provide a versatile solution by offering customized compliance. Acting as non-linear springs near the fairleads with adjustable stiffness, they reduce tension while keeping platform motion within acceptable limits. LDRs can be precisely tailored to environmental conditions and used with catenary or taut lines [7]. Therefore, automated optimization methods are required to effectively design these systems, considering all relevant variables.

To the best of our knowledge, no prior study has applied automated design optimization to nylon-based mooring systems that incorporate LDRs, specifically polymer springs. This paper presents a multi-objective cost optimization framework for such a system. The study simultaneously assessed LDR length and target load across various mooring line radii. A multi-objective framework, previously applied to optimize nylon-chain mooring systems, was chosen for two primary reasons: to assess its effectiveness for an LDR-nylon-chain system and to enable a cost comparison between the two systems. This study provides a detailed investigation of the relationship between design variables and mooring system radius, followed by an evaluation of the key dynamic behaviors of the optimal solutions for the smallest and largest radii.

The remainder of the paper is organized as follows: Section I introduces the context and background, Section II outlines the optimization framework. Section III describes the materials, model, and data environment. Section IV presents the results and discussion, and Section V concludes with recommendations for future work.

1.1. Mooring System Optimization Literature Review

Mooring optimization typically aims to identify the optimal line materials, lengths, and diameters to both enhance performance and reduce costs. Early studies relied on frequency-domain simulations (FDS). Shafieefar and Rezvani [8] focused on minimizing offsets for catenary chain-wire mooring systems under ultimate load conditions (ULS), while Brommundt et al. [9] reduced line length and costs for a catenary chain mooring on a floating offshore wind turbine (FOWT), considering ULS, platform movement, and seabed characteristics. Benassai et al. [10] lowered mooring mass in two FOWT catenary chain moorings while ensuring stability. Finally, Ferreira et al. [11] optimized truncated mooring parameters—line mass and diameter—using chain-wire and chain-polyester combinations to replicate full-depth mooring behaviour with time-domain simulations (TDS).

Optimization often employs simulation software to evaluate objective and constraint functions that are typically treated as black-box models. Surrogate models are used as substitutes to reduce computational effort. Li et al. [12] minimized the total cost of an offshore fish farm's single-point mooring by adjusting chain and wire rope dimensions, applying Kriging metamodels, TDS, and sequential quadratic programming (SQP). Pillai et al. [13] minimized fatigue damage and material costs in FOWT mooring systems by optimizing the use of chains and polyester ropes, combining a random forest (RF) surrogate model alongside the Non-dominated Sorting Genetic Algorithm II (NSGA-II) under tension limits and anchor constraints, and training the RF using TDS. Lim et al. [14] minimized the maximum mooring line tension for a polar oil platform using an artificial neural network (ANN) surrogate model with Bayesian optimization (BO) and a genetic algorithm (GA). BO was significantly more efficient, converging with 150 data points compared to GA's 3,120, and running approximately 20 times faster. Jiang et al. [15] minimized mooring system costs for a FOWT using an ANN and GA under platform acceleration, mooring tension, and motion constraints, training the ANN with TDS. While FDS can underestimate peak mooring loads by up to 50% [16], TDS is computationally intensive, and surrogate models may not be sufficiently accurate, necessitating trade-offs between accuracy and computational

cost. To address these challenges, West et al. [17] optimized a semi-taut nylon-chain mooring system for a shallow-water FOWT using NSGA-II. They aimed to minimize costs across various mooring radii, mitigating computational intensity by approximating mean loads, applying cascading constraints to eliminate infeasible designs, and performing approximate TDS only on promising configurations.

Most mooring systems studied to date have incorporated chain, chain-wire, and chain-synthetic lines. Early work on LDR mooring systems includes the study by Festa et al. [18], who examined a chain catenary mooring integrated with a polymer spring LDR for a FOWT. They used polynomial and cubic regression surrogate models to minimize tension and surge. Aryawan et al. [19] contrasted traditional steel wire moorings with ground chains to nylon-based systems with polymer spring LDRs for FOWTs, using dynamic TDS under ULS constraints without employing optimization tools. Additionally, Festa et al. [7] optimized LDR designs to diminish tension and surge in chain catenary and chain-synthetic taut systems for FOWTs, demonstrating that optimal polymer spring LDR designs require robust, multivariate analyses.

1.2. Polymer Spring Technology Literature Review

Festa et al. [7] describe the polymer spring developed by Technology for Ideas (TFI) as a mooring component composed of compressive polymer materials, designed to reduce peak dynamic loads on floating structures. The device features a dual-phase design that begins with a low-stiffness, regressive-load response, allowing significant elongation of the mooring line under normal conditions and thereby improving system compliance. When the load reaches the rated tension, steel flanges inside the device engage ("lock-out"), shifting the spring to a high-stiffness phase that curtails further elongation, thus ensuring structural integrity under extreme conditions.

McEvoy and Kim [20] effectively utilized these polymer springs in floating tidal devices, demonstrating their potential for reducing dynamic mooring loads. Further analyses on FOWT mooring systems by Aryawan et al. [19] and Lozon et al. [21] demonstrated that polymer springs not only reduce maximum mooring loads but also prolong fatigue life, reduce the mooring footprint, optimize platform motion, and yield significant cost savings in installation, operation, and maintenance. These savings may reduce the levelized cost of energy (LCOE), enhancing the economic attractiveness of the technology.

Polymer springs can be customized to exhibit specific stress-strain response curves. This paper focuses on a degressive axial stiffness design of the polymer spring, as illustrated in Figure 1. The spring's response is defined by its "target load," which is the tension corresponding to approximately 50% compression or elongation—as illustrated by a 5,000 kN target load in Figure 1. Figure 2(a) depicts the typical mooring load-excursion behaviour of a FOWT under wave, wind, and current forces, showing that the mooring line remains stiff near the turbine's thrust load. By judiciously selecting appropriate polymer spring response curves and target loads, as well as adjusting the number or size of the spring components, peak mooring loads can be significantly reduced. Figure 2(b) illustrates how the spring, designed to be stiff at lower tensions and more compliant at higher loads improves the overall mooring system performance.

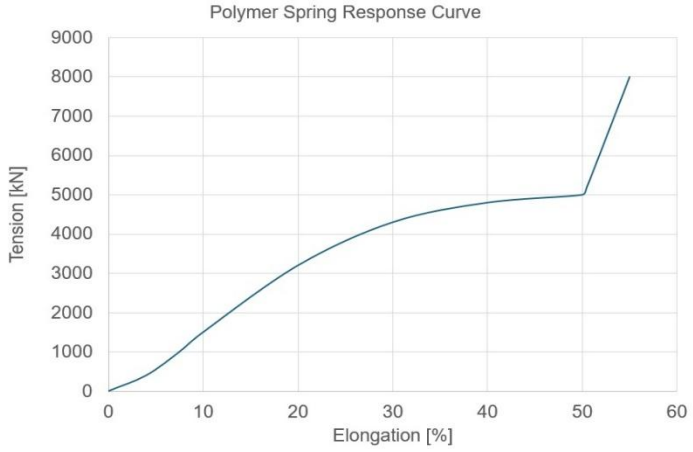

Figure 1. Example of polymer spring Tension - Elongation curve

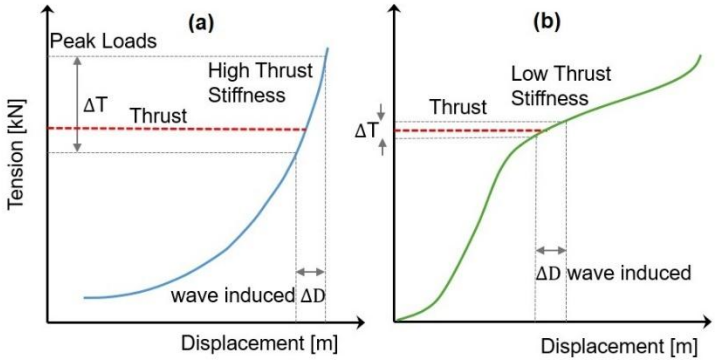

Figure 2. Illustration of FOWT Mooring Load Behavior

II. OPTIMIZATION FRAMEWORK

This study adopts an optimization framework similar to that introduced by West et al. [17], with modifications implemented to meet the specific requirements of our analysis. It utilizes the Non-Sorted Genetic Algorithm II (NSGA-II) [22] to identify a Pareto front that minimizes costs while maximizing mooring system radii.

2.1. Termination Criteria

The "running metric", a relatively recent method proposed by Blank and Deb [23], is employed to analyze optimization runs when the true Pareto front is unknown. Typically, multi-objective algorithms aim to improve convergence based on dominance relations or solution set diversity. The running metric capitalizes on this by monitoring indicators related to extreme points and the non-dominated solution set in each generation, thereby producing measures of convergence and diversity. The open-source optimization framework pymoo uses this metric to terminate a multi-objective optimization routine when predefined criteria are not specified. Three parameters must be defined: "tol," which is the allowable difference between specific metrics of non-dominated solutions in consecutive generations; "period," which is the final number of generations for analysis; and "skip," which is the number of excluded generations. For more details, refer to Blank and Deb [23].

2.2. Multi-Objective Optimization Problem for Identifying Minimum-Cost Designs Across Various Mooring Radii

In a multi-objective optimization, the objective functions must compete; otherwise, the solutions could converge to a single point. Mooring radii and cost are not inherently competitive in a mooring system incorporating a Load Reduction Device (LRD). To ensure that these objectives are indeed competitive, we map the mooring system radius and cost onto competing criteria, as suggested by West et al. [17]. The optimization problem, including constraints, is formulated mathematically as follows:

$$
\begin{aligned}
&Maximize\ -L(\boldsymbol{x})\ and\ \varphi(\boldsymbol{x}) \\
&Subject\ to\ g_i(\boldsymbol{x}) \geq 0, i = 1,2,\dots 8 \\
&R_{min} \leq R \leq R_{max} \\
&L_{syn_{min}} \leq L_{syn} \leq L_{syn_{max}} \\
&L_{spr_{min}} \leq L_{spr} \leq L_{spr_{max}} \\
&D_{chain_{min}} \leq D_{chain} \leq D_{chain_{max}} \\
&D_{syn_{min}} \leq D_{syn} \leq D_{syn_{max}} \\
&V_{min} \leq V \leq V_{max} \\
&TL_{min} \leq TL \leq TL_{max}
\end{aligned}
\qquad \text{Eq. (1)}
$$

The symbols are defined in Table 1, and the constraints are briefly discussed in Section 2.2.2.

Table 1. Design Variables and Their Ranges

Design variable	Description	Variable Type	Range
R	Mooring system radius	Continuous	250 m – 400 m
L_{syn}	Length of the nylon line (as fraction of radius)	Continuous	0.4 – 0.61 (100 m – 244 m)
L_{spr}	Length of the spring (as fraction of radius)	Continuous	0.02 – 0.04 (5 m – 16 m)
d_{chain}	Diameter of the chain line	Continuous	135 mm – 178 mm
d_{syn}	Diameter of the nylon line	Continuous	175 mm – 240 mm
V	Buoy displaced volume	Continuous	0 m^3 – 10 m^3
TL	Target load of the spring component	Continuous	3,000 kN – 6,000 kN

2.2.1. Objective Function

To establish two competing objectives, we map the mooring radius and mooring system cost as suggested by West et al. [17]. For each feasible design, we define a vector that originates from a cost of zero and the lower bound of the selectable radii. The objective is to shorten the length of this vector, guiding the optimizer toward more cost-effective designs, while maximizing the vector's angle to maintain a diverse set of solutions along the front. Equations (2) and (3) present the mathematical formulation of the objective functions. The cost is standardized to ensure a suitable range of variation in both the vector length and angle:

$$L(\boldsymbol{x}) = \sqrt{(C(\boldsymbol{x})/M_{norm})^2 + (R - R_{min})^2} \quad \text{Eq. (2)}$$

$$\varphi(\boldsymbol{x}) = tan^{-1}\left(\frac{R - R_{min}}{C(\boldsymbol{x})/M_{norm}}\right) \quad \text{Eq. (3)}$$

where $C(\boldsymbol{x})$ denotes the total material cost of the mooring system, including the anchor, and M_{norm} is the normalization constant for the mooring cost.

2.2.2. Constraints

The hierarchical constraint approach introduced by West et al. [17] serves to eliminate design variables that violate specific requirements, thereby reducing the need for computationally intensive analyses. It operates as a cascade: the design moves through a series of layers, each representing a constraint function. A small constant, tailored to filter out marginally infeasible designs, is added to each constraint function. This constant diminishes as the design progresses through the layers. The following section briefly describes all the constraints. For detailed mathematical formulations, see West et al. [17].

The constraint $\boldsymbol{g_1(x)}$ filters out extreme designs where mooring line lengths are not feasible. The constraints $\boldsymbol{g_2(x)}$, $\boldsymbol{g_3(x)}$, and $\boldsymbol{g_4(x)}$ identify designs susceptible to resonance issues, which can potentially influence the time-domain response of the platform.

The constraint $\boldsymbol{g_5(x)}$ ensures that the nylon line does not contact the seabed, while the constraints $\boldsymbol{g_6(x)}$ and $\boldsymbol{g_7(x)}$ ensure that the tension in chain and nylon lines can withstand dynamic loading. Finally, the constraint $\boldsymbol{g_8(x)}$, used specifically for the LDR-chain-nylon mooring system, encourages the algorithm to select a spring capable of reducing the maximum line tensions to or below its target load, as expressed by the following equation:

$$g_8 = \begin{cases} 3\dfrac{T_{fairlead_{max}} - T_{target\ load}}{T_{target\ load}}, & if\ T_{fairlead_{max}} \geq T_{target\ load} \\ 0 & otherwise \end{cases} \quad \text{Eq. (4)}$$

where $T_{fairlead_{max}}$ denotes the maximum tension at the fairlead. It is important to highlight that the last three constraints are evaluated through expensive time-domain simulations.

III. MATERIAL, MODELS AND METHODS

The following sections provide a brief outline the inputs, adapted from West et al. [17], used for conducting the optimization in this study.

3.1. Mooring System

The mooring system geometry subjected to optimization is shown in Figure 3. Its constant properties, as well as the stiffness and the MBL of the chain and nylon lines, are available in West et al. [17]. The synthetic lines feature a specific gravity of 1.15 g/cm³, and the steel chain has a mass density of 8050 kg/m³. Table 2 displays the load-elongation lookup table implemented in OrcaFlex:

$$c = Target\ Load/2{,}500 \qquad \text{Eq. (5)}$$

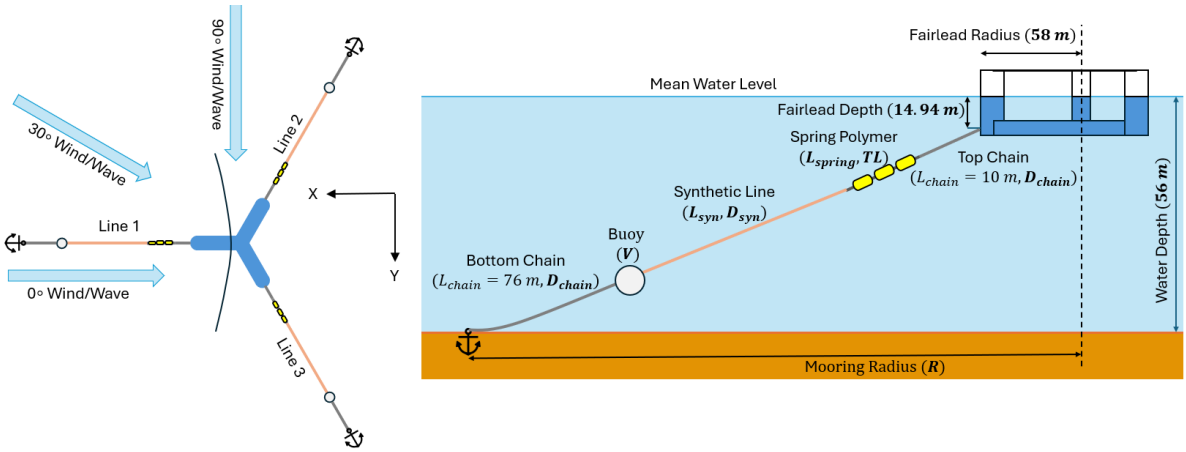

Figure 3. Mooring System Geometry and LDR

Table 2. Lookup table varying with the target load

Elongation [%]	0	5	10	15	20	25	30	35	40	45	50	55
Tension [kN] x10²	0	5·c	9·c	12·c	16·c	19·c	21·c	22·c	24·c	24.5·c	25·c	42·c

The linear mass of the spring is estimated using data from Lozon et al. [21], where a spring with a target load of 4,000 kN exhibits a linear mass of 1,759.9 kg/m. The spring's linear mass can be determined using the following equation:

$$linear\ mass = \frac{1{,}759.9}{4{,}000} Target\ Load \qquad \text{Eq. (6)}$$

The default OrcaFlex damping coefficients for the nylon line were applied to the LDR. The material cost data used to estimate the mooring cost are presented in Table 3. The cost of the LDR was obtained from McEvoy et al. [24].

Table 3. Mooring system component costs

Material	Cost (USD/kg)
Steel chain	1.5
Nylon	17
Buoy	22.3
Anchor	155
Spring	1.2 x 1.5 = 1.8
Mooring cost normalization constant	33,000

3.2. Other Components

To ensure a fair comparison, we also modelled the 15 MW Reference Turbine upon the submersible

platform Volturn US-S [25]. The system is anchored by the Vryhof Stevmantis Mk 5 drag embedment anchor [26]. A detailed mathematical description of the anchor is provided in West et al. [17].

3.3. Design Code Requirements

The design criteria, as discussed in West et al. [17], integrate ABS [27], API [28], and IEC [29] recommendations, along with previous findings from the University of Maine. The minimum chain safety factor accounts for 25-year DLC 1.2 fatigue conditions. The platform's natural period is kept out of the wave energy region, with heave and pitch periods of 18 s and 25 s. A surge period ranging from 55 to 350 s prevents the mooring system from becoming overly rigid or overly compliant. The synthetic mooring line remains suspended above the seafloor, and anchor sizing is carried out using conservative soil parameters. ABS specifies a minimum clearance of 1.0 m for the synthetic section, with larger clearances required for more conservative designs.

3.4. Environmental Condition

We considered two environmental conditions typical of a lease area near New York: the 50-year return period load case for a parked turbine [17] and the 50-year load case for an operating turbine [21]. This combination enables a fair comparison of the LDR-nylon-chain mooring system with the nylon-chain system analyzed by West et al. [17] and the LDR-chain system studied by Lozon et al. [21]. We applied combined 1st-order wave and mean 2nd-order wave, current, and wind loads to the platform to accelerate simulations and ensure computational feasibility during the optimization process, following West et al. [17]. Tables 4 and 5 summarize the environmental loading data at the FOWT site.

Table 4. ABS design parameters for environmental conditions

Feature	Load case	
	DLC 1.6 (50-yr operational)	DLC 6.1 (50-yr parked)
Significant wave height (m)	4.72	8.4
Peak wave period (s)	10.03	11.65
Peak shape parameter	2.02	3.09
Wind speed (m/s)	10.59	39
Turbulence intensity	0.085	0.154
Current (m/s)	Not considered	1.39

Table 5. Environmental Conditions Used for DCL 6.1 Optimization

Feature	Mean Load (kN)
1st wave effect (idem)	N/A
2nd order wave effect	64.2
Wind	896
Current	1780

3.5. Approach for Modelling the Extrapolation of Peak Loads

For synthetic lines, the ABS-recommended method employs quasi-static stiffness to determine system pretension and thereby evaluate the platform's mean offsets and mooring line tensions [27]. Dynamic simulations then utilize dynamic stiffness, adjusting the line length to match the quasi-static pretension. After this alignment, dynamic simulations are conducted, and response amplitudes are added to the static mean tension. A random design underwent six 1-hour simulations with different seeds, closely following the method developed by West et al. [17], to determine the average maximum tension according to the ABS method. Subsequently, 24 simulations of 1,000 s each were performed, with

maximum tension peaks fitted to a generalized extreme value (GEV) distribution to extrapolate the maximum tension. Seed 747140245 was chosen because it best matched the extrapolated and average tensions. A more precise dynamic analysis, incorporating Turbsim-generated turbulent wind inflow and configuring OrcaFlex for second-order wave effects, revealed that the approximate method underestimated maximum tension by up to 16%. For more details, refer to West et al. [30].

3.6. OrcaFlex set – up

To expedite the determination of mean offsets, we adjusted the linear and quadratic damping coefficients in the OrcaFlex input files, resulting in an overdamped system that stabilizes displacements and mooring line tensions more rapidly. For further details, see West et al. [30]. Table 6 summarizes the OrcaFlex settings used for both the mean offset simulations and the DLC 6.1 tension time history.

Table 6. OrcaFlex Line Section Discretization

OrcaFlex time step (s)	Top chain discretization (segments)	Spring section discretization (segments)	Synthetic section discretization (segments)	Bottom chain discretization (segments)
0.2	4	5	50	20

IV. RESULTS AND DISCUSSION

The NSGA-II optimization was performed using pymoo's default parameters, as detailed in Table 7. The Pareto fronts were obtained after 80 generations, using the running metric employed as the termination criterion. This significantly lowered computational costs compared to running 400 generations [17], which would have taken much longer. The parameters for the running metric are detailed at the bottom of Table 7. The entire simulation consumed 560,447 seconds (approximately 156 hours or 6.5 days).

Table 7. Parameters for NSGA-II

Parameter	Value
Population size	140
Crossover operator	Exponential
Crossover probability	0.9
Crossover distribution index (η)	15
Mutation operator	Exponential
Mutation probability	0.9
Mutation distribution index (η)	20
Elitism	Implicit to NSGA-II
Tolerance	0.05
Period	10
Skip	2

4.1. Objective Space Analysis

The Pareto fronts for both systems are presented in Figure 4. The nylon-chain mooring system optimized by West et al. [17] yielded costs between $1.25 and $1.4 million, while the mooring system with the LDR achieved significantly lower costs, ranging from $0.7 to $1.1 million. Table 8 shows that the average factor of safety (FoS) of the solutions is slightly above target, suggesting further reductions in the chain and nylon diameters could be possible. However, the algorithm is constrained by the fixed lower bound values for these diameters, preventing the selection of smaller sizes.

Table 8. Factor of Safety (FoS) Statistics

Material	Target FoS	Average FoS	Max FoS	Min FoS	FoS COV
Chain	3.30	3.47	3.90	3.38	2.21%
Synthetic	2.18	2.23	2.35	2.18	1.63%

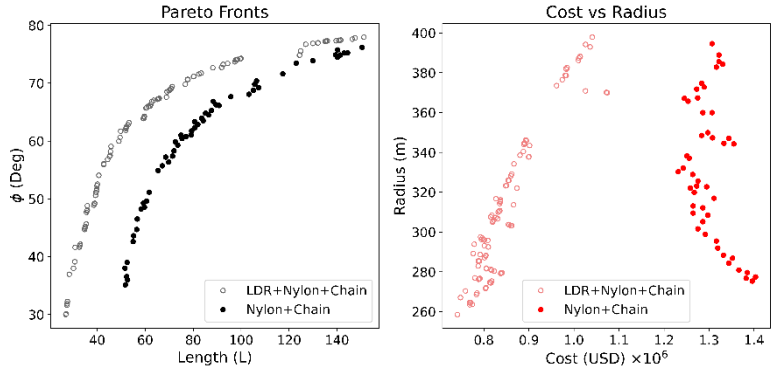

Figure 4. Pareto Fronts and Corresponding Mooring Radius vs. Cost Relationship

4.2. Design Space Analysis

The optimized design space offers valuable insights. Figure 5(a) shows that the target load varies from 3,630 to 4,011 kN, increasing as the radius decreases. This is expected, since smaller radii results in higher fairlead tension. Figure 5(b) shows spring lengths ranging from 6 to 12 m, increasing as the radius grows, indicating that the algorithm mitigates line tension by extending the spring length. Figure 5(c) illustrates that the buoy's displaced volume stabilizes at 1.5 m³, which is sufficient to keep the bottom chain off the seabed, making the mooring system taut. Figure 5(d) shows a positive correlation between mooring radius and synthetic line length, while Figures 5(e) and (f) indicate that both chain and synthetic diameters reached their lower bounds of 135 mm and 175 mm, respectively. This aligns with Festa [7], who noted that LDRs enable mooring systems not constrained by their physical or geometric properties.

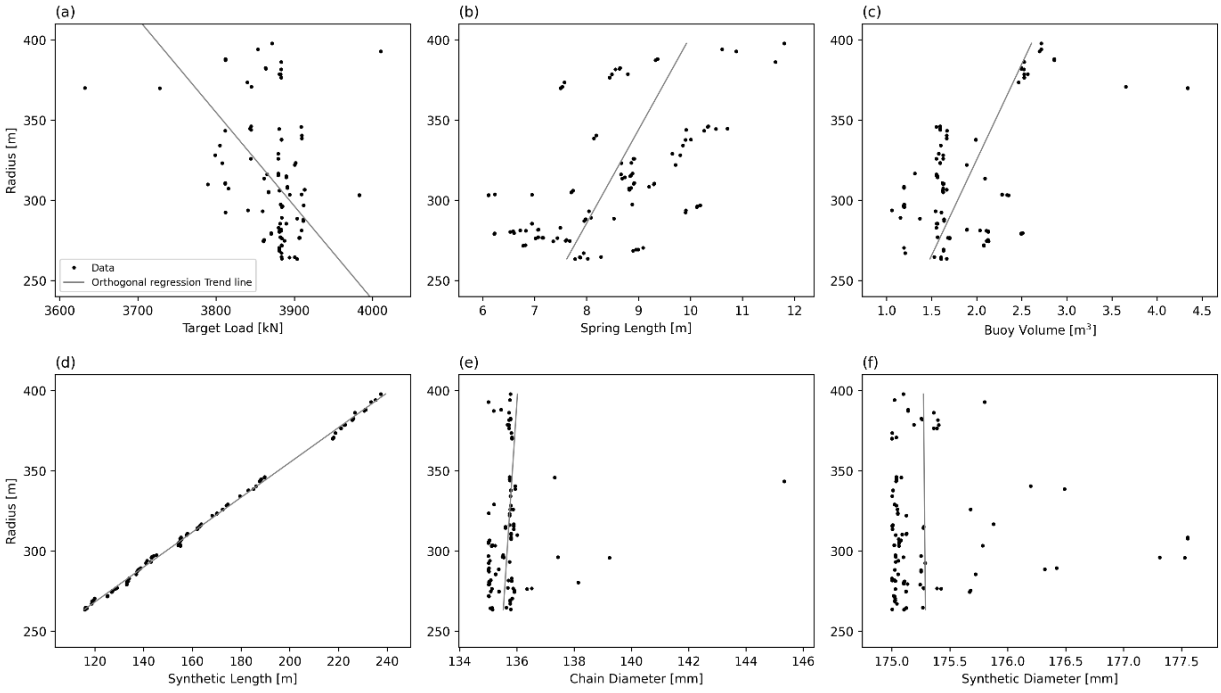

Figure 5. Radius vs (a) Target Load, (b) Spring Length, (c) Buoy Displaced Volume, (d) Synthetic Length, (e) Chain Diameter, (f) Synthetic Diameter.

4.3. Optimized Design Validation

Two optimized designs with the largest and smallest radii, shown in Table 9, were tested against full turbulent wind DLC 6.1 and DLC 1.6, with the latter including 0°, 30°, and 90° wind-wave headings to evaluate yaw angle.

Table 9. Optimized Design

Radius (m)	Synthetic Length (m)	Spring Length (m)	Chain Diam (mm)	Synthetic Diam (mm)	Buoy Displaced Volume (m^3)	Target Load (kN)
258	109	10	135	176	1.17	4024
398	237	12	135	175	2.71	3871

Table 10 summarizes the tension statistics, showing that the factors of safety (FoS) for both the chain and nylon materials fell slightly short of the target values, as expected due to the approximate method used for tension estimation. However, the differences are minor, and designers can easily adjust the chain and nylon diameters to meet code requirements. They can also select a spring stiffness curve with a target load slightly above the maximum tension. The damage equivalent load (DEL), representing the amplitude of a constant cyclic load that causes the same cumulative fatigue damage as an irregular loading time-series, was calculated using a rainflow counting algorithm with a fatigue slope of 5. The DEL for the chain diameter is about half of what Lozon et al. [21] reported for an LDR-chain mooring system with the largest radius.

Table 10. Tension [kN] Line 1 Statistic Summary

Radius (m)	Material	Min	Max	Mean	STD	MBL	MBL/Max	FoS	DEL
258	Chain	2058	4310	3313	372	13121	3.04	3.3	460
	Nylon	1999	4275	3265	377	8500	1.99	2.18	N/A
398	Chain	2677	4165	3466	228	13121	3.15	3.3	284
	Nylon	2635	4129	3431	232	8500	2.06	2.18	N/A

Table 11 summarizes platform motions and nacelle accelerations for both radii across the DLCs. The maximum surge of 19.1 m for the largest radius stays within the 20 m limit, consistent with the offset-to-water depth ratio used by Pillai et al. [5], which was 25/70 = 0.35. The maximum pitch remains below 6°, as suggested by Allen et al. [25], and the nacelle acceleration of 1.50 m/s² falls under the 0.2g threshold, where g is gravity acceleration.

Table 11. Platform Motions and Nacelle Accelerations

Radius	Features	DLC 6.1				DLC 1.6			
		Min	Max	Mean	STD	Min	Max	Mean	STD
398 m	Surge (m)	11.2	-19.1	-15.1	1.26	3.39	8.41	5.94	0.84
	Heave (m)	-1.15	2.53	0.61	0.63	-0.55	1.48	0.47	0.3
	Pitch (Deg)	-2.1	1.54	-0.12	0.54	1.32	5.02	0.32	0.63
	Yaw (Deg)	-1.76	1.20	-0.02	0.55	-1.3	2.06	0.189	0.56
	Nacelle accel. (m/s^2)	0.0049	1.42	0.39	0.21	0.0031	1.04	0.26	0.16
258 m	Surge (m)	7.32	-14.21	-10.84	1.11	-1.03	6	2.26	0.69
	Heave (m)	-1.18	2.52	0.59	0.63	-0.52	1.50	0.49	0.30
	Pitch (Deg)	-1.83	1.817	0.15	0.53	-4.92	-1.27	-3.07	0.62
	Yaw (Deg)	-1.81	1.84	0.06	0.65	-1.84	2.72	0.43	0.86
	Nacelle accel. (m/s^2)	0.0053	1.50	0.394	0.21	0.0026	0.99	0.26	0.16

Table 12 displays the yaw angle statistic for DLC 1.6, 30° and 90° wind-wave headings. The maximum yaw angle is much lower than 5°, at 2.21°.

Table 12. Yaw Angle (Deg) Statistic for a Mooring Radius of 398 m

DLC 1.6 30 wind - wave heading				DLC 1.6 90 wind - wave heading			
Min	Max	Mean	STD	Min	Max	Mean	STD
-1.78	2.21	0.19	0.62	-1.712	2.29	0.179	0.62

Figure 6 shows the time series and power density spectral response for both mooring systems under the DLC 6.1 case. In some platform motions and fairlead tensions, a power spectral peak near the wave frequency of 0.085 Hz is observed. Rigid body modal analysis of the platform, considering the static stiffness of the nylon rope, was performed for both systems to ensure that the primary mode frequencies did not coincide with the wave frequencies. Tables 13 and 14 show that the first ten mode shapes do not match the wave frequency. However, the narrow peaks in the power spectrum of platform motions and fairlead tension around 0.085 Hz, shown in Figure 6, indicate that system damping is likely very low, suggesting that more accurate damping coefficients for the LDR may improve the results.

Table 13. Modal Analysis for a Mooring Radius of 258 m

Mode Number	1	2	3	4	5	6	7	8	9	10
Period (s)	122.3	75.92	75.92	28.53	28.53	20.11	5.63	5.63	5.63	4.65
Frequency (Hz)	0.01	0.01	0.01	0.04	0.04	0.05	0.18	0.18	0.18	0.22

Table 14. Modal Analysis for a Mooring Radius of 398 m

Mode Number	1	2	3	4	5	6	7	8	9	10
Period (s)	84.75	75.77	75.77	28.21	28.21	20.13	5.53	5.53	5.53	5.4
Frequency (Hz)	0.01	0.01	0.01	0.04	0.04	0.05	0.18	0.18	0.18	0.19

V. CONCLUSIONS

This research addresses a key gap in the optimization of LDR-nylon-chain mooring systems by simultaneously considering critical LDR parameters—length, target load, and stiffness—within a unified multi-objective framework. By adapting an existing approach originally developed for nylon-chain systems, we successfully applied it to LDR-nylon-chain configurations and demonstrated significant cost reductions for both small and large platform radii. The Pareto fronts derived under the new optimization strategy revealed that beyond approximately 1.5 m^3 of buoy volume—sufficient to maintain the nylon line above the seabed—the system becomes effectively taut, with nylon and chain diameters reaching their lower bounds, confirming that the LDR dominates mooring stiffness characteristics. Dynamic simulations lasting 3,600 seconds (DLC 6.1 and 1.6) validated these findings, showing that target load and spring length could be fine-tuned without compromising motion performance or nacelle acceleration limits. Although fatigue damage was also reduced, the low system damping, attributed to the LDR, warrants further investigation. Moreover, slight exceedances in allowable mooring line tension indicate that while the proposed algorithm provides a robust initial design, final configurations must still be verified against regulatory codes; however, such adjustments can be quickly implemented to ensure compliance. The entire optimization process required approximately 6.5 days on a standard notebook, a duration that could be substantially reduced with enhanced computational resources. Future work should focus on refining LDR damping coefficients, incorporating viscoelastic models for nylon lines, and exploring alternative LDRs and anchoring solutions. Such improvements could prove especially beneficial in wind farm environments, where shared anchors may unlock additional optimization opportunities.

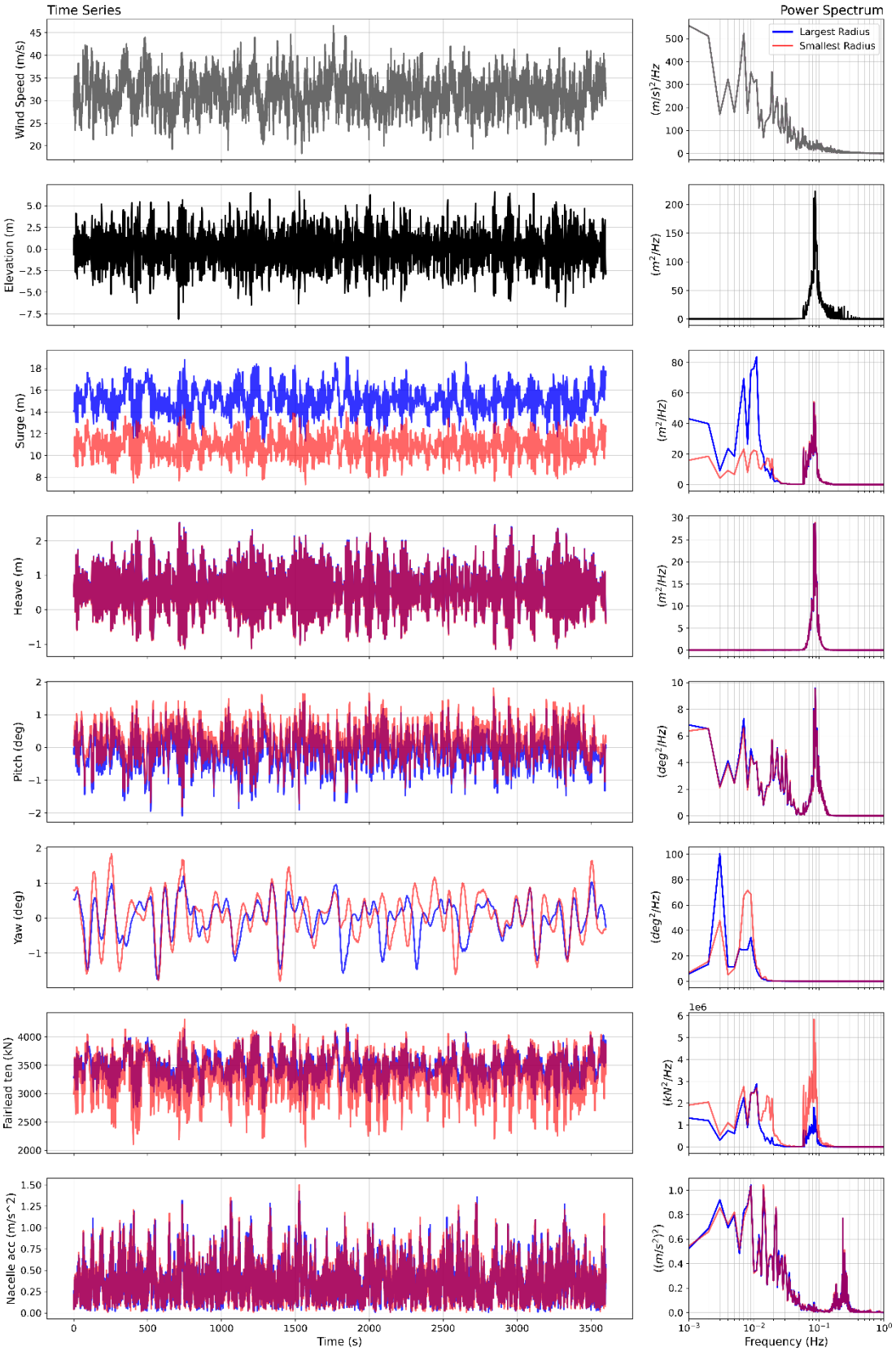

Figure 6. DLC 6.1 Time Series and Power Density Spectral Response

ACKNOWLEDGEMENTS

The authors acknowledge the Laboratory of Scientific Computing and Visualization (LCCV) at the Center of Technology (CTEC), Federal University of Alagoas (UFAL), for its support of this research.

The second author acknowledges the support of the Brazilian National Council for Scientific and Technological Development (CNPq) in the development of this work.

REFERENCES

[1] R. Williams, A. Martinez Palacio, and F. Zhao, "GLOBAL OFFSHORE WIND REPORT." Accessed: Jan. 24, 2024. [Online]. Available: https://gwec.net/wp-content/uploads/2023/08/GWEC-Global-Offshore-Wind-Report-2023.pdf

[2] Gov.br, "Portal vai unificar tramitação de empreendimentos de energia offshore." Accessed: Jan. 24, 2024. [Online]. Available: https://www.gov.br/pt-br/noticias/energia-minerais-e-combustiveis/2022/10/portal-vai-unificar-tramitacao-de-empreendimentos-de-energia-offshore

[3] Empresa de Pesquisa Energética, "Roadmap Eólica Offshore Brasil." Accessed: Jan. 24, 2024. [Online]. Available: https://www.epe.gov.br/sites-pt/publicacoes-dados-abertos/publicacoes/PublicacoesArquivos/publicacao-456/Roadmap_Eolica_Offshore_EPE_versao_R2.pdf

[4] K. Xu, K. Larsen, Y. Shao, M. Zhang, Z. Gao, and T. Moan, "Design and comparative analysis of alternative mooring systems for floating wind turbines in shallow water with emphasis on ultimate limit state design," *Ocean Engineering*, vol. 219, p. 108377, Feb. 2020, doi: 10.1016/j.oceaneng.2020.108377.

[5] A. C. Pillai, T. J. Gordelier, P. R. Thies, D. Cuthill, and L. Johanning, "Anchor loads for shallow water mooring of a 15 MW floating wind turbine—Part II: Synthetic and novel mooring systems," *Ocean Engineering*, vol. 266, Dec. 2022, doi: 10.1016/j.oceaneng.2022.112619.

[6] S. Verde and E. N. Lages, "A comparison of anchor loads, planar displacement, and rotation for nylon and polyester moored systems for a 15 MW floating wind turbine in shallow water," *Ocean Engineering*, vol. 280, Jul. 2023, doi: 10.1016/j.oceaneng.2023.114404.

[7] O. Festa, S. Gourvenec, and A. Sobey, "Comparative analysis of load reduction device stiffness curves for floating offshore wind moorings," *Ocean Engineering*, vol. 298, Apr. 2024, doi: 10.1016/j.oceaneng.2024.117266.

[8] M. Shafieefar and A. Rezvani, "Mooring optimization of floating platforms using a genetic algorithm," *Ocean Engineering*, vol. 34, no. 10, pp. 1413–1421, Jul. 2007, doi: 10.1016/j.oceaneng.2006.10.005.

[9] M. Brommundt, L. Krause, K. Merz, and M. Muskulus, "Mooring system optimization for floating wind turbines using frequency domain analysis," in *Energy Procedia*, Elsevier Ltd, 2012, pp. 289–296. doi: 10.1016/j.egypro.2012.06.111.

[10] G. Benassai, A. Campanile, V. Piscopo, and A. Scamardella, "Optimization of Mooring Systems for Floating Offshore Wind Turbines," *Coastal Engineering Journal*, vol. 57, no. 4, Dec. 2015, doi: 10.1142/S0578563415500217.

[11] F. M. G. Ferreira, E. N. Lages, S. M. B. Afonso, and P. R. M. Lyra, "Dynamic design optimization of an equivalent truncated mooring system," *Ocean Engineering*, vol. 122, pp. 186–201, 2016, doi: 10.1016/j.oceaneng.2016.06.021.

[12] L. Li, Z. Jiang, M. C. Ong, and W. Hu, "Design optimization of mooring system: An application to a vessel-shaped offshore fish farm," *Eng Struct*, vol. 197, Oct. 2019, doi: 10.1016/j.engstruct.2019.109363.

[13] A. C. Pillai, P. R. Thies, and L. Johanning, "Mooring system design optimization using a surrogate assisted multi-objective genetic algorithm," *Engineering Optimization*, vol. 51, no. 8, pp. 1370–1392, Aug. 2019, doi: 10.1080/0305215X.2018.1519559.

[14] J. Lim, M. Choi, and S. Lee, "A Bayesian Optimization Algorithm for the Optimization of Mooring System Design Using Time-Domain Analysis," *J Mar Sci Eng*, vol. 11, no. 3, Mar. 2023, doi: 10.3390/jmse11030507.

[15] Y. Jiang, Y. Duan, J. Li, M. Chen, and X. Zhang, "Optimization of mooring systems for a 10MW semisubmersible offshore wind turbines based on neural network," *Ocean Engineering*, vol. 296, Mar. 2024, doi: 10.1016/j.oceaneng.2024.117020.

[16] M. Hall and A. Goupee, "Validation of a lumped-mass mooring line model with DeepCwind semisubmersible model test data," *Ocean Engineering*, vol. 104, pp. 590–603, Jun. 2015, doi: 10.1016/j.oceaneng.2015.05.035.

[17] W. M. West, A. J. Goupee, S. T. Hallowell, and A. M. Viselli, "Determination of minimum-cost synthetic mooring systems for large floating wind turbines deployed in intermediate water depths," *Journal of Renewable and Sustainable Energy*, vol. 15, no. 1, Jan. 2023, doi: 10.1063/5.0123474.

[18] O. Festa, S. Gourvenec, and A. Sobey, *Proxy model for the design of extensible floating offshore wind turbine mooring systems*. 2022. [Online]. Available: http://onepetro.org/ISOPEIOPEC/proceedings-pdf/ISOPE22/All-ISOPE22/ISOPE-I-22-030/2788459/isope-i-22-030.pdf/1

[19] I. Aryawan, P. McEvoy, S. Kim, and R. P. Faria, "Potential Mooring System Optimization Using Polymer Spring Component – Floating Offshore Wind Turbine Application," in *Proceedings of the Annual Offshore Technology Conference*, Offshore Technology Conference, 2023. doi: 10.4043/32410-MS.

[20] P. Mcevoy and S. Kim, "Mooring load management for SR2000 floating tidal device using non-linear polymer components.," 2017. Accessed: Sep. 28, 2023. [Online]. Available: https://uploads-ssl.webflow.com/5f8964a5a533790d6cc8820a/5f96cb7a8ba32845a778cb9e_EWTEC-2017.pdf

[21] E. Lozon, M. Hall, P. Mcevoy, S. Kim, and B. Ling, "Design and Analysis of a Floating-Wind Shallow-Water Mooring System Featuring Polymer Springs. In: ASME 2022 4th International Offshore Wind Technical. Ocean, Offshore and Arctic Engineering Division.," 2022. doi: 10.1115/IOWTC2022-98149.

[22] K. Deb, A. Pratap, S. Agarwal, and T. Meyarivan, "A Fast and Elitist Multiobjective Genetic Algorithm: NSGA-II," *IEEE Trans. Evol. Comput.*, vol. 6, no. 2, pp. 182–197, 2002, doi: 10.1109/4235.996017.

[23] J. Blank and K. Deb, "A Running Performance Metric and Termination Criterion for Evaluating Evolutionary Multi-and Many-objective Optimization Algorithms.," in *IEEE Congress on Evolutionary Computation (CEC).*, Glasgow, UK.: IEEE, Jul. 2020. doi: 10.1109/CEC48606.2020.9185546.

[24] P. McEvoy, E. Johnston, and T. Marine, "Polymer Mooring Component for Offshore Renewable Energy. In Offshore Technology Conference.," Houston, Texas, USA, 2019. doi: 10.4043/29587-MS.

[25] C. Allen *et al.*, "Definition of the UMaine VolturnUS-S Reference Platform Developed for the IEA Wind 15-Megawatt Offshore Reference Wind Turbine.," *Golden CO: National Renewable Energy Laboratory. NREL/TP-5000-76773*, 2020. [Online]. Available: www.nrel.gov/publications.

[26] Vryhof, *VRYHOF MANUAL: THE GUIDE TO ANCHORING*. 2018. [Online]. Available: https://vryhof.com/vryhof-anchors/

[27] ABS, "Requirements for Position Mooring Systems.," 2023, *ABS: Spring, TX, USA*.

[28] API, "Design and Analysis of Stationkeeping Systems for Floating Offshore Structures," 2018, *API: Washington, DC, USA*.

[29] IEC, "IEC 61400–3 Design Requirements for Offshore Wind Turbines," 2019, *IEC: Geneve, Switzerland.*

[30] W. West, A. Goupee, S. Hallowell, and A. Viselli, "Development of a Multi-Objective Optimization Tool for Screening Designs of Taut Synthetic Mooring Systems to Minimize Mooring Component Cost and Footprint," *Modelling*, vol. 2, no. 4, pp. 728–752, Dec. 2021, doi: 10.3390/modelling2040039.

Authors

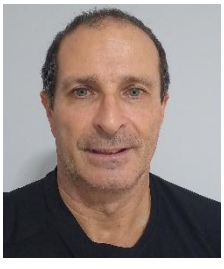

Salvatore Verde: He earned a Bachelor's degree in Civil Engineering from the University of Naples Federico II in 1997, followed by a Master of Science in Structural Engineering from the Graduate Program in Structural Engineering at the Federal University of Bahia (UFBA) in 2014. In 2024, he completed a Ph.D. in Civil Engineering with a focus on Structures and Materials from the Graduate Program in Civil Engineering (PPGEC) at the Federal University of Alagoas (UFAL). Currently, he serves as an Associate Professor at UFAL. His primary areas of expertise include offshore construction, computational mechanics, fluid dynamics, and steel structures.

Eduardo Nobre Lages: He earned a Bachelor's degree in Civil Engineering from the Federal University of Alagoas (UFAL) in 1989, followed by a Master's degree in 1992 and a Ph.D. in 1997, both in Civil Engineering with a concentration in Structures from the Pontifical Catholic University of Rio de Janeiro (PUC-RJ). He is a Full Professor at the Center of Technology (CTEC) at the Federal University of Alagoas (UFAL). He is a permanent faculty member of the Graduate Program in Civil Engineering (PPGEC/CTEC/UFAL) and a researcher/coordinator at the Laboratory of Scientific Computing and Visualization (LCCV/CTEC/UFAL).